ADSORPTION OF 2-THIOURACIL AT THE MERCURY/ELECTROLYTE INTERFACE II. CAPACITANCE TRANSIENTS

Thomas WANDLOWSKI and Robert de LEVIE

Chemistry Department,
Georgetown University, Washington DC 20057, U.S.A.

Received May 7, 1992
Accepted July 18, 1992

Dedicated to Professor Václav Horák on the occasion of his 70th birthday.

The adsorption of 2-thiouracil at the mercury–water interface exhibits several regions. In region I, the capacitance is consistently higher than that of the supporting electrolyte, as is usually observed for sulfur-containing compounds. At higher concentrations of 2-thiouracil, two additional adsorption regions appear. Region II corresponds to a condensed monolayer, formed by nucleation and two-dimensional growth, while region III exhibits behavior typical for polylayer formation.

Sulfur-containing organic compounds play a special role in electrochemistry, in that they often exhibit unusual adsorption behavior. Much recent research has been devoted to chemisorptive "self-assembly" of thio-compounds on gold and platinum electrodes, but sulfur-containing compounds also show strong adsorption at the mercury–water interface. A prime example of such behavior is that of 2-thiouracil, a therapeutic agent used in the treatment of hyperthyroidism, angina pectoris and congestive heart failure, which forms an unusually stable condensed film at the mercury–water interface. While most condensed monolayer films are observable only at or below room temperature, the condensed film of 2-thiouracil can persist[1] up to at least 85 °C.

Previous investigations have shown that 2-thiouracil, dissolved in aqueous solutions of controlled pH, is adsorbed at mercury[1 - 3] and silver[4,5] electrodes. In a thermodynamic study[1] of 2-thiouracil adsorption on mercury from an aqueous 0.5 M NaF solution at pH 7 we distinguished three types of adsorption, denoted by I, II and III respectively, see Fig. 1. State I describes adsorption typical of sulfur-containing compounds, predominates at relatively low adsorbate concentrations and, at higher concentrations of 2-thiouracil, persists at strongly negative potentials. At high adsorbate concentrations, a condensed film is formed, labeled II. At even higher adsorbate concentrations, a second capacitance pit appears at positive potentials, here labeled III.

The previous paper[1] emphasized the static behavior of 2-thiouracil adsorption. In the present communication, we will augment this with information regarding the dynamic

behavior of 2-thiouracil adsorption, again at the interface between mercury and an aqueous 0.5 M NaF solution at pH 7, by reporting on capacitance transients.

EXPERIMENTAL

The solutions were made from pyrodistilled water, NaF (Merck Suprapur), and 10 mM phosphate buffer (Sigma), adjusted to pH 7. All supporting electrolyte solutions were treated with activated charcoal. The adsorbate, 2-thiouracil (Sigma), was used without further purification. The solutions were deoxygenated with nitrogen before the measurements.

The measurements were made on a PAR 303 hanging mercury electrode. Mercury droplets of 2.6 mm^2 area were formed at the end of an unsiliconized glass capillary. A saturated calomel electrode was used as reference, connected to the cell solution via a double-junction salt bridge. All potentials refer to this reference electrode. Most experiments were made using a 2-thiouracil concentration of 3.125 mmol l^{-1}, and at a temperature of 5.0 °C.

Capacitance measurements were made with a 1.59 kHz sinewave of 2.5 mV amplitude, superimposed on a voltage ramp or step. Positive feedback just short of oscillatory instability was used for compensation of the solution resistance. The alternating current was amplified, phase-selectively rectified with a lock-in amplifier, digitized and stored in a 80286-based computer. Further details of the measuring equipment can be found in ref.[6].

RESULTS

Capacitance–Potential Curves

Figure 1 shows a typical set of C–E curves (C capacitance, E potential) for 3.125 mM 2-thiouracil in 0.5 M NaF + 10 mM phosphate buffer at pH 7 and 5.0 °C, and will serve to identify the different adsorption states, I through III. The adsorbate concentration was sufficiently high to reduce diffusion-related time dependencies to negligible levels.

Two different voltage scan rates were used, and the scan was made in both directions. The dependence of the capacitance on scan rate indicates that these are not equilibrium curves. This applies especially to the regions around the transitions I $\rightleftharpoons$ II and II $\rightleftharpoons$ III, which exhibit strong hysteresis between the positive- and negative-going voltage scans. We note that region III is skipped altogether at the higher scan rate.

Capacitance Transients for the Formation of State II

Figure 2 shows a set of C–t transients (t time) following single potential steps starting from E_0 = –1.600 V to potentials in region II near its negative edge. When E_0 is made less negative, the shapes of these sigmoid curves are independent of the initial potential, and of the time t_0 spent at E_0, as long as E_0 remains in region I.

The transients can be analyzed by converting the measured capacitance C into a fractional film coverage Θ using

$$\Theta = \frac{C_I - C}{C_I - C_{II}} , \qquad (1)$$

where C_I and C_{II} are the initial and final capacitance values respectively. The fractional coverage can be described quantitatively by combining the Canac–Avrami equation

$$\Theta = 1 - e^{-\Theta_X} , \qquad (2)$$

where Θ_X is the extended fractional coverage, with a rate expression of the form

$$\Theta_X = b t^m . \qquad (3)$$

The inset in Fig. 2 shows the corresponding Avrami plots of $\ln \ln [(C_I - C_{II})/(C - C_{II})] = \ln \Theta_X$ versus $\ln t$. The resulting plots are essentially linear, in accordance with Eq. (3), and have slopes m in the range from 2.9 to 3.1.

We have used double potential step experiments to determine the time dependence of film growth. Starting at E_0 = –1.600 V, we jumped to E_1 = –0.835 for a period t_1 of up

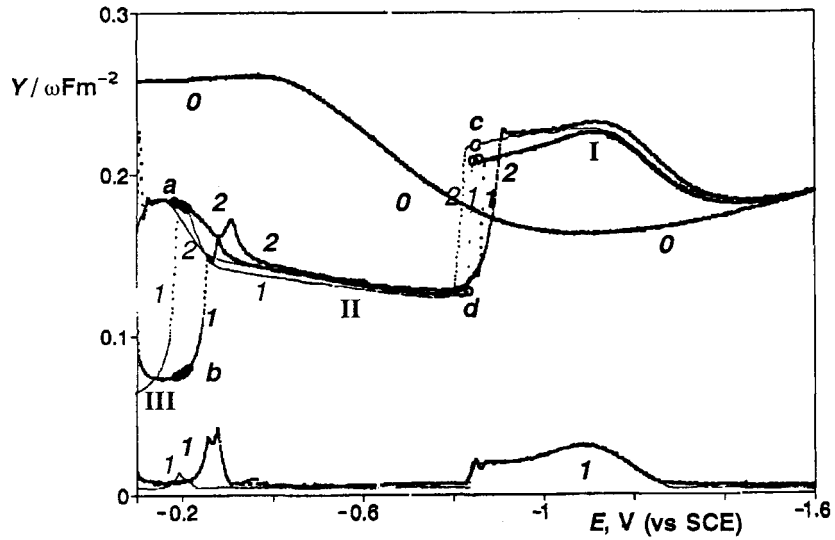

FIG. 1

Capacitance–potential curves for mercury in contact with aqueous 0.5 M NaF + 10 mM phosphate buffer pH 7 (curve ***0***) and the same plus 3.125 mM 2-thiouracil, all at 5 °C. The heavy curves ***1*** and ***2*** were recorded with the potential moving towards more negative potentials whereas, for the thin curves *1* and *2*, the potential was scanned in the positive direction. Magnitude of the scan rates: 5 m V s^{-1} for curves ***1***, *1*; 500 m V s^{-1} for curves ***2***, *2*. (Curve ***0*** is independent of scan rate or scan direction.) The bottom curves display the corresponding in-phase components of measured signal. Circles show the initial (***a***, ***c***) and final (***b***, ***d***) capacitance values of single potential step experiments from –0.3 V into region III (***a***, ***b***) and from –1.6 V into region II (***c***, ***d***)

to 0.24 s, long enough to form a number of nuclei yet too short for growth to cover more than a small fraction of the surface. We then stepped to the potential E_2 = −0.865 V, where nucleation was slow yet growth of nuclei pre-formed at E_1 continued, and where growth could therefore be studied in the absence of simultaneous nucleation.

Figure 3 illustrates the resulting transients measured at E_2. Note that no transient response is obtained when $t_1 = 0$, i.e., in absence of pre-nucleation. Avrami analysis of the resulting transients yielded linear curves of $\ln \Theta_x$ vs $\ln t$, with slopes of the order of *2*, see the insert of Fig. 3.

The above results of single-step and double-step experiments show that the kinetics of formation of the 2-thiouracil monolayer in region II are governed by progressive nucleation and rate-limiting two-dimensional growth. This explains a slope of *3* in the single-step experiments (in which the rate of nucleation is proportional to t, and the rate of growth to t^2, for a combined proportionality of Θ_X to t^3), and a slope *2* in the double-step experiments (in which the nuclei are preformed at E_1, leaving Θ_X to be proportional to t^2).

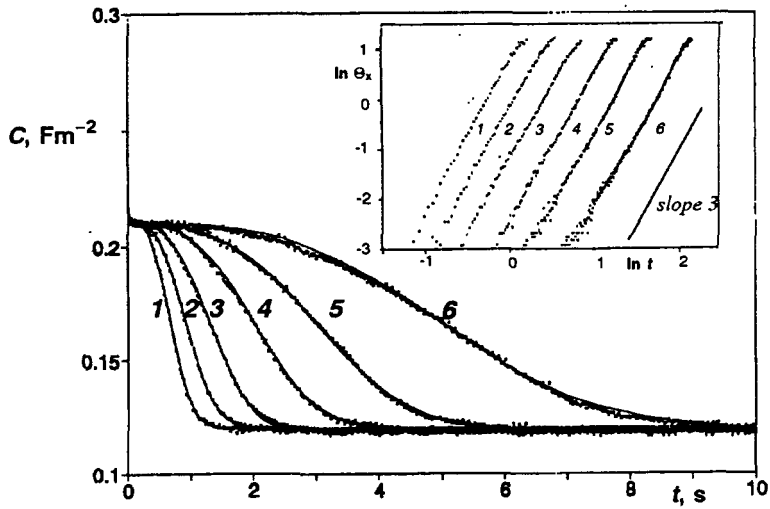

FIG. 2

Capacitance transients following single potential steps from E_0 = −1.600 V to −0.845 V (*1*), −0.846 V (*2*), −0.847 V (*3*), −0.848 V (*4*), −0.849 V (*5*), −0.850 V (*6*). The lines through the measured points were drawn according to Eqs (*1*) through (*3*) with m = 3.0, i.e., with only one adjustable parameter, the intercept b. They illustrate the degree of agreement between experiment and theory. The inset shows the corresponding Avrami plots of $\ln \Theta_X$ vs $\ln t$. Unweighted linear least squares analyses of these Avrami plots yield slopes of *3.00*, *3.10*, *2.90*, *3.04*, *3.02* and *2.90* for curves *1* through *6* respectively

The thin lines drawn in Fig. 2 show a comparison of the experimental transients with those calculated from Eq. (*1*) through Eq. (*3*) with m = 3.0, i.e., with only b as adjustable parameter.

Similar capacitance transients, both in the central part of region II and at its positive edge, were faster than could be resolved reliably with our present equipment.

Capacitance Transients for the Formation of State III

Figure 4 shows the capacitive transients for a set of single step experiments at 5 °C with variable starting potential E_0 and fixed final potential E_1 = −0.150 V, i.e., in region III. Also shown are the corresponding in-phase components of the response. When we start from the "bare" electrode surface, at $E_0 \leq -1.6$ V, identical curves are found regardless of the value of E_0. Transients following steps from region II, i.e., from −0.4 V $\leq E_0 \leq$ −0.8 V, are likewise independent of the precise value of E_0, but tend to lower capacitance values. Finally, when the voltage step originates from region I, i.e., from between −0.9 and −1.6 V, the transients systematically change depending on the value of E_0, as it were making a continuous transition between the transients for $E_0 \leq -1.6$ V

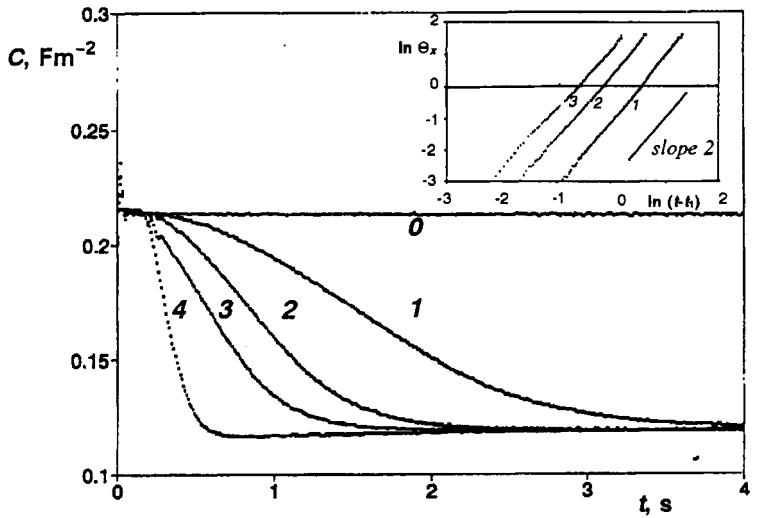

FIG. 3

Capacitance transients following a double potential step, first from E_0 = −1.600 V to E_1 = −0.835 V for t_1 = 0 ms (***0***), 12 ms (***1***), 18 ms (***2***) and 24 ms (***3***), followed by a step to E_2 = −0.865 V. Curve ***0*** demonstrates that no growth occurs at −0.865 V in the absence of preceding nucleation. Curve ***4*** shows a transient resulting from a single potential step from −1.600 V to −0.835 V, showing that growth at −0.835 V is relatively insignificant during the initial 12 to 24 ms. The inset shows the resulting Avrami plots for curves *1* through *3*, and (for comparison) a line drawn under slope *2*

and $E_0 \geq -0.8$ V. Finally, we note that none of these transients reach well-defined final capacitance values.

In Fig. 5 we show some transients following single potential step from the very edge of region II into region III, i.e., from $E_0 = -0.3$ V to potentials more positive than −0.203 V. Immediately after the potential step, the capacitance rises to a metastable value, which corresponds to that observed in Fig. 1 at the higher (0.5 V s^{-1}) scan rate. Subsequently, the transients decay at a rate dependent on the value of the final potential E_1. For comparison, the initial and final capacitance values are shown as circles ***a*** and ***b*** in Fig. 1. (For the final values we have taken those reached 40 s after the voltage step.) The absence of a final capacitance value in region III suggests the formation of a polylayer.

By increasing the temperature to 20 °C, we can discriminate two types of transients, as illustrated in Fig. 6. One type has a fixed final value, while the other appears not to have one, similar to our observations at 5 °C. The curves leading to a well-defined final capacitance value yield approximately linear plots of ln $(1/(1 - \Theta))$ vs time t, as shown in the insert of Fig. 6. This can be described formally in terms of slow adsorption kinetics[7].

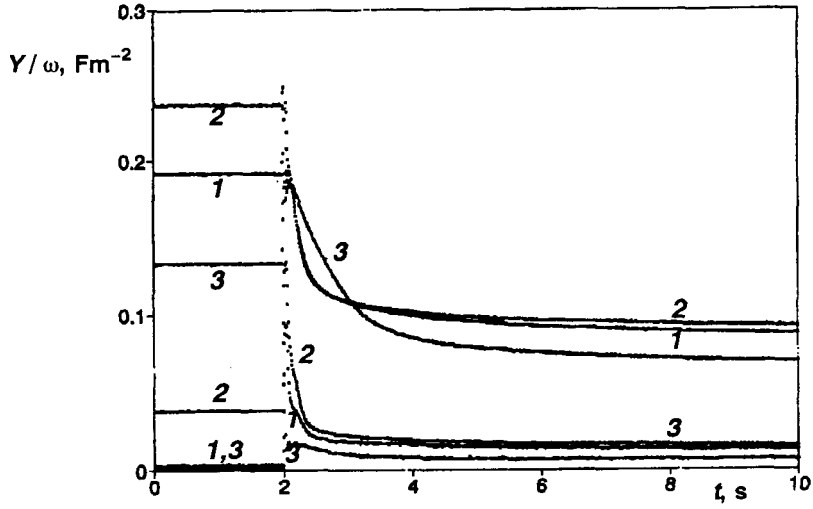

FIG. 4

Capacitance transients following a single potential step to $E_1 = -0.815$ V from $E_0 = -1.600$ V (***1***), $E_0 = -1.100$ V (***2***) and $E_0 = -0.600$ V (***3***) respectively. The bottom curves show the corresponding in-phase responses

Capacitance Transients for the Dissolution of State II

Figure 7 shows the final transients in double potential steps from −1.6 V to region II, as then to just past the boundary between II and I. Such transients depend on the value of the final potential E_1, and can be described approximately by

$$C = C_I + (C_{II} - C_I)\, e^{-kt} \qquad (4)$$

as illustrated in the inset. Such transients, gradually rising from the starting capacitance and asymmptotically approaching their final value, are believed to reflect slow desorption kinetics[7,8].

However, double potential step experiments, starting at E_0 = −1.6 V, jumping to E_1 = −0.8 V and staying there for a variable time t_1 before stepping to a final potential E_2 of −0.875 V, show that these transients change with the age of the film formed at E_1, as demonstrated in Fig. 8. We do not know whether this aging of the film, which is not reflected in a measurable capacitance change, depends on a physical process, such as annealing of domain boundaries, or on a chemical change, such as perhaps resulting from protolysis.

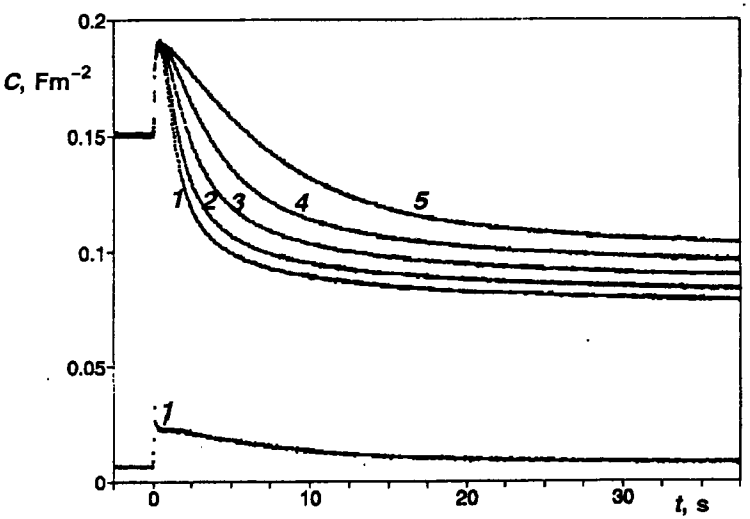

FIG. 5

Capacitance transients following single potential steps from E_0 = −0.300 V to E_1 = −0.186 V (*1*), −0.190 V (*2*), −0.194 V (*3*), −0.198 V (*4*) and −0.202 V (*5*). The bottom shows the corresponding transient of the in-phase component of Y/ω for E_1 = −0.186 V. Note that these transients do not appear to reach a steady-state. Circles in Fig. 1 show the capacitance values at the maximum in the transients (labeled *a*), and those reached after t_1 = 40 s (labeled *b*)

Capacitance Transients for the Dissolution of State III

Quite different desorption transients are observed when starting from region III. In that case, the capacitance responds to an applied voltage step by a sudden change to a new value, followed by a transient which often goes through a maximum before settling down to its final value. Figures 9 and 10 depict such behavior. We believe that the steep initial capacitance change is caused by fast desorption, which releases a large surplus of adsorbate in the adjacent solution. The subsequent transient then results from the establishment of a transient adsorption equilibrium between the (temporarily enhanced) sub-surface concentration and the interface, while the surplus adsorbate slowly diffuses away towards the bulk solution[8,9].

Such transient behavior is observed only when the final potential E_1 is near the edges of region II, where the equilibrium interfacial excess Γ varies with the sub-surface concentration; when E_1 is chosen to be in the central part of region II, the capacitance steps immediately to its final value, since the capacitance at those potentials is virtually independent of concentration (as long as the latter is high enough to sustain the condensed monolayer). Note that the capacitance maxima in the transients of Fig. 9 are accompanied by an equally large resistive component, attesting to their diffusional

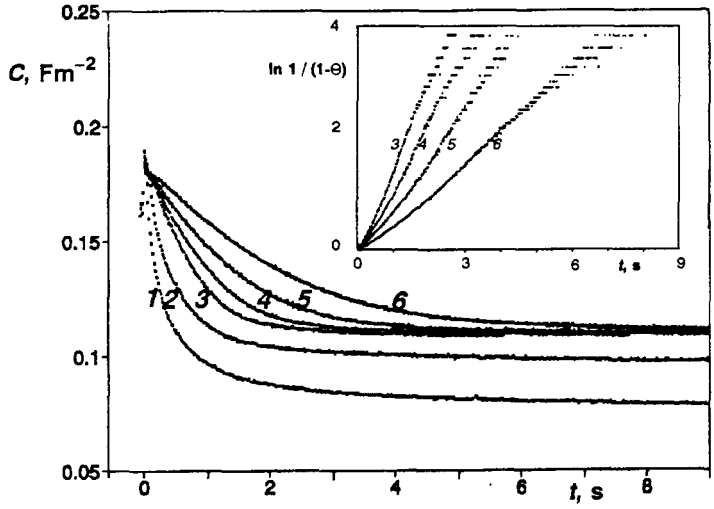

FIG. 6

Capacitance transients, at 20 °C, following single potential steps from E_0 = −0.500 V to E_1 = −0.140 V (*1*), −0.170 V (*2*), −0.200 V (*3*), −0.205 V (*4*), −0.210 V (*5*) and −0.215 V (*6*). Note that curves *3* through *6* now converge to a similar final value. The inset shows ln (1/(1 − Θ)) as a function of time t after the potential step

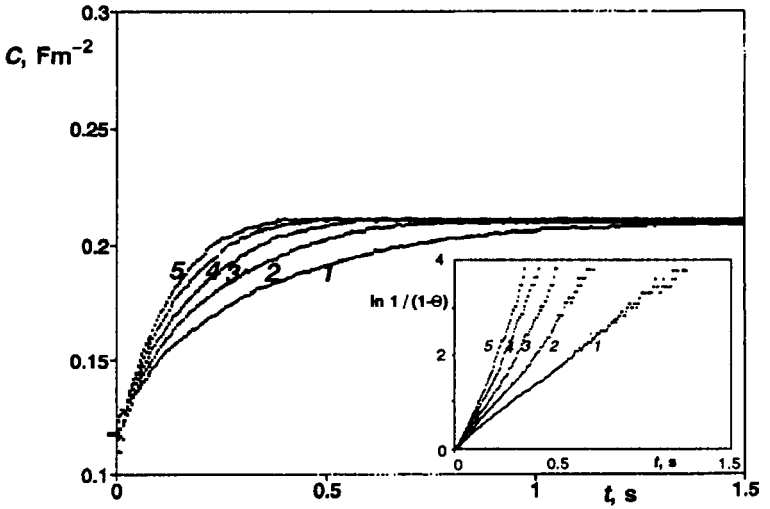

FIG. 7

Capacitance transients following double potential steps, first from E_0 = -1.600 V to E_1 = -0.830 V and, after 1 s there, on to -0.876 V (*1*), -0.877 V (*2*), -0.878 V (*3*), -0.879 V (*4*) and -0.880 V (*5*). The inset shows the same data plotted as ln (1/(1 – Θ)) vs *t*

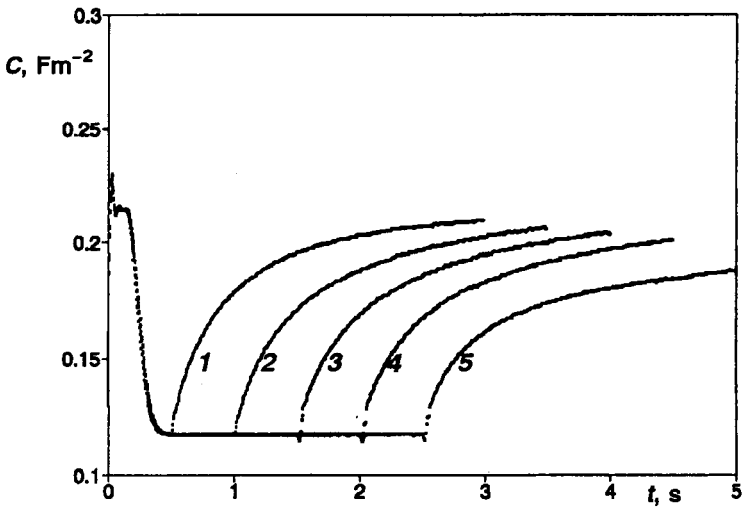

FIG. 8

Capacitance transients following double potential steps, first from E_0 = -1.600 V to E_1 = -0.800 V and, after a variable time t_1, on to -0.875 V. The following residence times t_1 at -0.800 V were used: 0.5 s (*1*), 1.0 s (*2*), 1.5 s (*3*), 2.0 s (*4*) and 2.5 s (*5*)

nature: a Warburg impedance also has in-phase and quadrature components of equal magnitude.

The transients in Fig. 10 suggest that desorption in that case occurs in three separate stages. First, the capacitance rises quickly (i. e., instantaneously as far as our equipment is concerned) to the capacitance of region II. Subsequently, the capacitance goes through a maximum, and this is followed by an increase to the final capacitance, corresponding to adsorption in region I. In this case, the in-phase component of the transient maximum is larger than its capacitive component, implicating the presence of a slow adsorption process. However, this qualitative interpretation is a provisional one, pending a quantitative analysis of these quite complicated transients.

DISCUSSION

The capacitance transients accompanying the formation of region II clearly show nucleation and two-dimensional growth as their rate-determining processes. In the double potential step measurements, nuclei are preformed at E_1, and the subsequent transient reflects the growth of these nuclei. Such experiments yield the time-dependence of monolayer growth, although they do not lead to a numerical value for the rate constant because the number of preformed nuclei is not known. Given the time-depend-

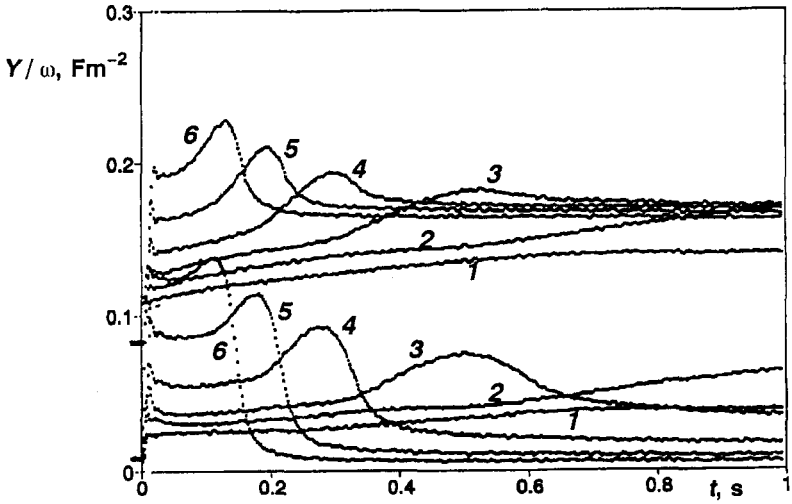

FIG. 9

Capacitance transients following double potential steps, first from E_0 = −1.600 V to E_1 = −0.150 V and, after 5 s there, on to −0.240 V (*1*), −0.260 V (*2*), −0.280 V (*3*), −0.300 V (*4*), −0.320 V (*5*) and −0.340 V (*6*). The top curves show the capacitive (quadrature) components of the transients, the bottom their resistive (in-phase) parts

ence of growth, the single step experiments then show that the rate of nucleation is directly proportional to time, i.e., without an appreciable induction delay. Again, deterministic experiments such as described here only yield qualitative information; stochastic observations would be needed in order to obtain specific nucleation rate constants.

Our results for state II conform with those on other purines and pyrimidines, which can form well-defined condensed monolayers at the mercury–water interface[10]. This is noteworthy only insofar as the adsorption in region I is unlike that of most purines and pyrimidines, but is instead characteristic for sulfur-containing molecules, with a capacitance higher than that of the supporting electrolyte. In that sense, our observations are akin to those on thiourea[11 - 13].

The apparent aging of the monolayer II has its counterparts in similar observations at the mercury–water interface[14,15] and, of course, in observations on silver monolayers on silver single crystal surfaces[16 - 18].

The transients accompanying the formation and dissolution of state III suggest that state III is a polylayer. We want to emphasize here that state III does not involve mercury oxidation; the latter occurs at more positive potentials, and is associated with the formation of sulfur-containing mercury compounds[19,20].

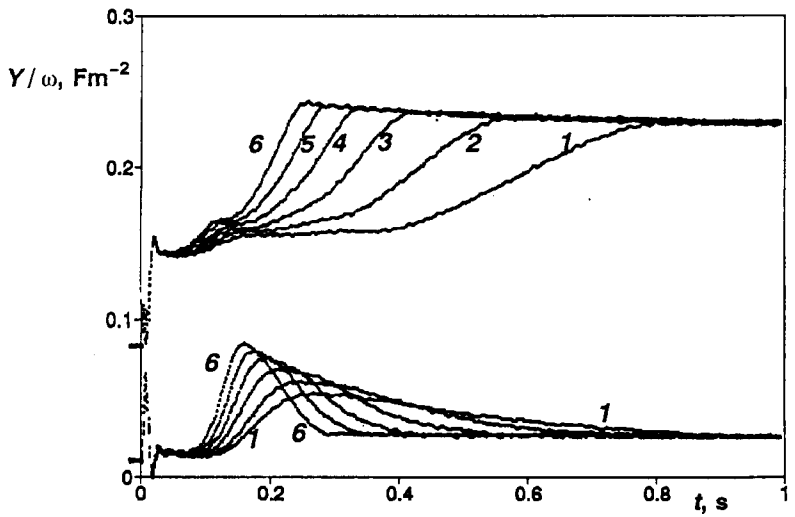

FIG. 10

Capacitance transients following double potential steps, first from E_0 = −1.600 V to E_1 = −0.150 V and, after 5 s there, on to −0.875 V (*1*), −0.880 V (*2*), −0.885 V (*3*), −0.890 V (*4*), −0.895 V (*5*) and −0.900 V (*6*). Again, the top curves show the capacitive (quadrature) components of the transients, and the bottom their resistive (in-phase) parts

We gratefully acknowledge financial support from NSF under grant CHE-8921563.

REFERENCES

1. Wandlowski T.: J. Electroanal. Chem. *312*, 245 (1991).
2. Wrona M.: J. Electroanal. Chem. *155*, 169 (1983).
3. Wandlowski T., Kretschmer E., Müller E., Kuschel F., Hoffmann S., von Lipinski K. J.: J. Electroanal. Chem. *213*, 339 (1986).
4. Hepel M., Osteryoung R. A.: J. Electroanal. Chem. *149*, 193 (1983).
5. Hepel M., Osteryoung R. A.: J. Electroanal. Chem. *160*, 217 (1984).
6. Sridharan R., de Levie R.: J. Electroanal. Chem. *201*, 133 (1986).
7. Lorenz W., Möckel F.: Z. Elektrochem. *60*, 939 (1956).
8. de Levie R., Vogt A.: J. Electroanal. Chem., in press.
9. Kurtyka B., Kaisheva M., de Levie R.: J. Electroanal. Chem., in press.
10. de Levie R.: Chem. Rev. *88*, 599 (1988) and references therein.
11. Schapink F. W., Oudeman M., Leu K. W., Helle J. N.: Trans. Faraday Soc. *56*, 415 (1960).
12. Meurée N., Gierst L.: Collect. Czech. Chem. Commun. *36*, 389 (1971).
13. Buess-Herman C., Gierst L., Gonze M., Silva F.: J. Electroanal. Chem. *226*, 267 (1987).
14. Pospíšil L.: J. Electroanal. Chem. *206*, 269 (1986).
15. Wandlowski T., Pospíšil L.: J. Electroanal. Chem. *258*, 179 (1989).
16. Bostanov V.: J. Crystal Growth *42*, 194 (1977).
17. Bostanov V., Obretenov W., Staikov G., Roe D. K., Budevski E.: J. Crystal Growth *52*, 761 (1981).
18. Obretenov W., Bostanov V., Popov V.: J. Electroanal. Chem. *132*, 273 (1982).
19. Manoušek O., Zuman P.: Collect. Czech. Chem. Commun. *20*, 1340 (1955).
20. Paleček E., Jelen F., Hung M. A., Lasovsky J.: J. Electroanal. Chem. *128*, 621 (1981).